
**Separation Science and Technology**
Publication details, including instructions for authors and subscription information:
http://www.informaworld.com/smpp/title~content=t713708471

# Modelling of Weak Acid Conversion in an EDl Cell

Frédéric Schab[ab]; Laurence Muhr[a]; Roda Bounaceur[a]; Marc-André Théoleyre[b]; Georges Grévillot[a]
[a] Laboratoire des Sciences du Génie Chimique - Nancy-Université - CNRS - ENSIC, Nancy, France [b] Applexion-Novasep - Novasep Process - 5, Chemin du Pilon, Saint Maurice de Beynost - F-01708, Miribel, France

Online publication date: 06 May 2010

**To cite this Article** Schab, Frédéric , Muhr, Laurence , Bounaceur, Roda , Théoleyre, Marc-André and Grévillot, Georges(2010) 'Modelling of Weak Acid Conversion in an EDl Cell', Separation Science and Technology, 45: 8, 1015 — 1024
**To link to this Article: DOI:** 10.1080/01496391003727882
**URL:** http://dx.doi.org/10.1080/01496391003727882

*Separation Science and Technology*, 45: 1015–1024, 2010

ISSN: 0149-6395 print/1520-5754 online
DOI: 10.1080/01496391003727882

Taylor & Francis
Taylor & Francis Group

# Modelling of Weak Acid Conversion in an EDl Cell

**Frédéric Schab,[1,2] Laurence Muhr,[1] Roda Bounaceur,[1] Marc-André Théoleyre,[2] and Georges Grévillot[1]**

[1]*Laboratoire des Sciences du Génie Chimique – Nancy-Université – CNRS – ENSIC, Nancy, France*
[2]*Applexion-Novasep – Novasep Process – 5, Chemin du Pilon, Saint Maurice de Beynost – F-01708, Miribel, France*

**The modelling of weak acid conversion in an EDl cell is described. The model takes into account the solution and resin ion transport numbers, acid dissociation, and ion exchange equilibrium. Simulations, which provide results that agree well with experiments, enable us to evaluate concentrations and conductivities in each position of the ion exchange packed bed, leading to 2D representations. A reduced flow rate $F_{red}$, defined as the ratio of the experimental flow rate over the maximum flow rate which would enable 100% conversion, in the case of 100% current efficiency, has been introduced. Steady-state conversion rate appears to have a strong nonlinear dependency on this dimensionless parameter.**

**Keywords** current efficiency; electrodeionization; electrodialysis; ion exchange; organic acid



## INTRODUCTION

Electrodeionization (EDl) is a hybrid technique, combining ion exchange and electrodialysis. Different EDI concepts have been developed, with homopolar or bipolar membranes (1). Using ion exchange resins enables the extension of electrodialysis application field to the case of dilute solutions. Indeed, electrodialysis limits are due to the high resistivity of the ion-depleting compartment once low concentrations are reached. Introduction of ion-exchange media in this compartment enables the lowering of resistivity, as ion-exchangers are more conductive than the treated solution. EDI can therefore be considered a polishing treatment and its current application is ultrapure water production. However, this technique appears to have many other potential uses such as technologies for organic processes. The present work concerns weak acid conversion, from the acid salt into the acid form. This operation is industrially achieved using bipolar membrane electrodialysis (EDBM) (2–3). However, some applications, e.g., lactic acid for biopolymers elaboration (4) require high purity organic acid and EDI polishing process can then be used to attain higher conversion rates. When EDBM and EDI processes are to be used consecutively, transition must be carried out once solution conductivity becomes lower than ion exchange conductivity. This concentration range is investigated in the present study.

Different works were devoted, on the one hand, to modelling of weak acid production by EDBM method (5,6) and, on the other hand, to modelling of ultrapure water production by the EDI method (7,8) but, to our knowledge, no report has been published on modelling of weak acid production by the EDI method. The present paper deals with the modelling of an EDI compartment allowing the conversion of salt of weak acid into the corresponding acid.

## EXPERIMENTAL

In order to check the validity of the proposed model with experimental results, measures were performed with a laboratory EDI unit.

### Principle of the EDI System

The principle of the EDI experimental system is depicted in Fig. 1. Salt solution is fed through an ion exchange bed laid between two ion exchange membranes; on the cathodic side (−), a cation exchange membrane (CEM) is used whereas on the anodic side (+) two configurations are possible, one using CEM and the other using a BM (bipolar membrane). In the first case the process is denoted as EDI whereas in the second EDI-BM will be used.

Let us first consider EDI configuration: under the influence of an external electrical field, protons are transferred through the membranes from the anodic side towards the central compartment and sodium ions from the central compartment towards the cathodic side. Weak acid salt is therefore converted into its acid form in the central compartment. Depending on the conversion rate, ions

Received 30 March 2009; accepted 8 February 2010.
Address correspondence to Laurence Muhr, Laboratoire des Sciences du Génie Chimique – Nancy-Université – CNRS – ENSIC – LSGC – 1, rue Grandville – BP 20451 – F-54001 Nancy, France. Tel.: +33 (0)3 83 17 53 11; Fax: +33 (0)3 83 32 29 75. E-mail: Laurence.Muhr@ensic.inpl-nancy.fr

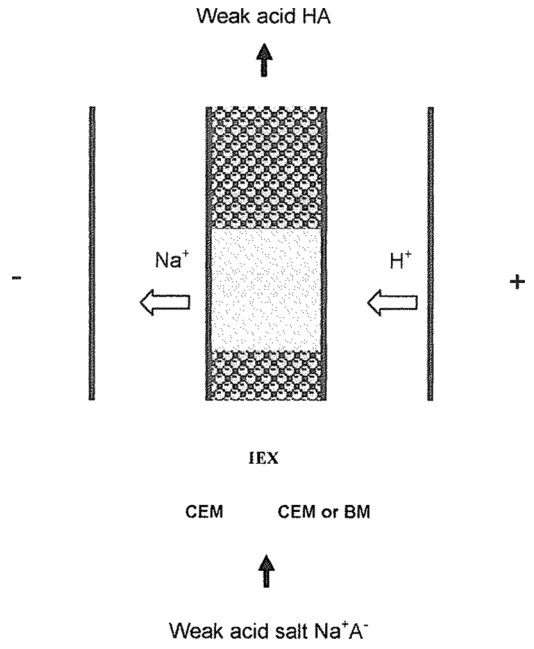


FIG. 1. Experimental EDI cell description. IEX: Ion Exchange Resin – CEM: Cation Exchange Membrane – BM: Bipolar Membrane.



transport through the bed occurs mainly via the solution or via the ion exchanger: as conversion proceeds solution conductivity decreases and the role played by ion exchange resins becomes predominant.

EDI-BM differs from the previous case only by the origin of protons, which are not transferred through the membrane from the anodic side but are generated by water splitting in BM.

The present modelling approach is focused on phenomena which take place within the ion-exchange packed bed: configuration choice will therefore have an influence on boundary conditions namely current densities which are implied in both cases.

All experiments and simulations are carried out using a "single pass" method, that is, without recycling the output flow in the feed.

### Materials and Chemicals

The thickness of the central compartment was 15 mm. This compartment was filled with a strong cationic resin. This resin was Amberlite 252 (Rohm and Haas), a macroporous styrene-DVB resin having a total capacity of 1.79 eq $L^{-1}$. The contact area of each membrane was $2 \times 20\,cm^2$. CEM was Nafion 117 (Dupont de Nemours), a strong cation exchange membrane, and BM was BP-1 (Tokuyama Soda). The anodic and cathodic compartments near the electrodes were 15 mm thick. Both electrodes were platinum coated titanium grids. Experiments presented hereafter were carried out in the case of the conversion of sodium lactate into lactic acid. Feed solutions were prepared with sodium lactate D/L-30%-synthetic origin (Sigma ©). These solutions were 0.125 (±0.005) N. This concentration corresponds to the isoconductivity point, that is, when the bed conductivity is equal to solution conductivity. The feed solution flowed continuously, in a single-pass way, through the central compartment.

## DEVELOPMENT OF THE MODEL

### Assumptions

Basic phenomena which are taken into account are:

- convection in the flow direction
- migration through the fixed bed
- acid dissociation and ion exchange equilibrium

Some phenomena are assumed to be negligible:

- diffusion is considered to have low influence compared to migration
- lateral convection is neglected. It must be noted that, for shallow beds, it would be preferable to take into account this phenomenon (1,8).
- ion transport through the membranes is considered to be a non-limiting step
- ideal selectivity of the cation exchange membranes is assumed. It can, however, be noticed that, in practice, EDI is often limited by insufficient anion rejection of the cation exchange membranes.
- hydroxyl ions contribution to the current transport is neglected as far as acidic media are considered.
- the change in solution volume due to water osmosis and electro-osmosis has not been taken into account
- due to ion exchange resins presence near the membranes, phenomena which occur in boundary layer in ED case, such as those caused by ion depletion, are not taken into account here.

### Cell Representation

The fixed bed compartment is divided into M*N cells (Fig. 2). M is the number of cells from one membrane to the other, N is the number of cells from bed input to bed output. Each cell is considered to have uniform concentrations. Each cell is indicated according to its coordinates (m, n), n being the line number and m the column number.

If S corresponds to each membrane area, the area of each cell in the vertical direction is:

$$S_c = S/N$$

If F is the flow rate which is fed through the fixed bed, flow rate through each cell is

$$F_c = F/M$$

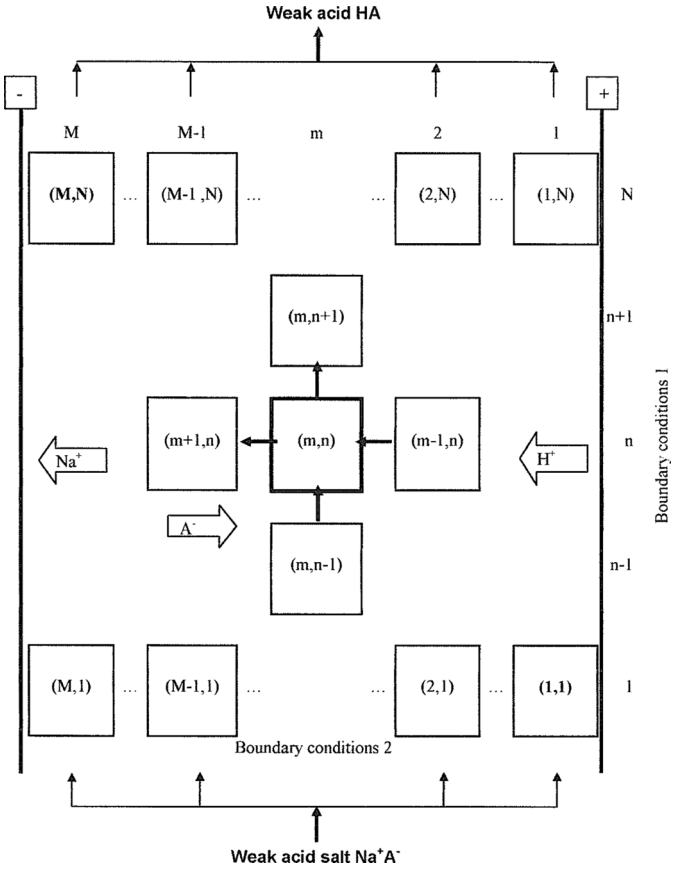


FIG. 2. Multi-compartment model used to describe the EDI cell.

## Problem Variables

The description of the model is made by the mean of several parameters as described below:

1. The following species are taken into account:
   - In liquid phase the concentration, noted C, of all ionic species: $H^+$, $Na^+$, $A^-$ (weak base), AH (weak acid) → 4 species
   - On cation exchange resin the concentration, noted q, of cationic species: $H^+$, $Na^+$ → 2 species
2. Conductivity in each cell $\kappa_{cell}$ is determined as a function of these concentrations. The transport number, noted t, is the fraction of the current carried by each ion that is present in solution. It is important to note that the sum of transport numbers in a solution should give one, $\sum t_+ + \sum t_- = 1$ where $\sum t_+$ and $\sum t_-$ are the sum of the transport number for cations and anions respectively.

Current is assumed to be constant along each horizontal line: N values $I_{line}$ are therefore considered. The sum of these N values is equal to the global current I. A single value of potential difference U is considered for the all system. The choice between two working modes is allowed: constant U or constant I.

Hence, for each cell, ten variables are determined: $C_{H+}$, $C_{Na+}$, $C_{A-}$, $C_{AH}$, $q_{H+}$, $q_{Na+}$, $\kappa_{cell}$, $t_{H+}$, $t_{Na+}$, $t_{A-}$

Transport numbers of ionic species, in each cell, are given by

$-\mathrm{Na}^+$

$$t_{Na^+}(m,n) = \frac{|z_{Na^+}|\overline{u_{Na^+}}, q_{Na^+}(m,n) + |z_{Na^+}|u_{Na^+}C_{Na^+}(m,n)}{|z_{Na^+}|\overline{u_{Na^+}}, q_{Na^+}(m,n) + |z_{Na^+}|u_{Na^+}C_{Na^+}(m,n) + |z_{H^+}|\overline{u_{H^+}}(Q - q_{Na^+}(m,n)) + |z_{H^+}|u_{H^+}C_{H^+}(m,n) + |z_{A^-}|u_{A^-}C_{A^-}(m,n)} \quad (1)$$

where $z$ is the valence number, $u$ the mobility in liquid phase, $\bar{u}$ the mobility in solid phase and $Q$ the resin capacity

$-\mathrm{A}^-$

$$t_{A^-}(m,n) = \frac{|z_{A^-}|\overline{u_{A^-}}C_{A^-}(m,n)}{|z_{Na^+}|\overline{u_{Na^+}}, q_{Na^+}(m,n) + |z_{Na^+}|u_{Na^+}C_{Na^+}(m,n) + |z_{H^+}|\overline{u_{H^+}}(Q - q_{Na^+}(m,n)) + |z_{H^+}|u_{H^+}C_{H^+}(m,n) + |z_{A^-}|u_{A^-}C_{A^-}(m,n)} \quad (2)$$

$-\mathrm{H}^+$

$$t_{H^-}(m,n) = \frac{|z_{H^+}|\overline{u_{H^+}}, q_{H^+}(m,n) + |z_{H^+}|u_{H^+}C_{H^+}(m,n)}{|z_{Na^+}|\overline{u_{Na^+}}, q_{Na^+}(m,n) + |z_{Na^+}|u_{Na^+}C_{Na^+}(m,n) + |z_{H^+}|\overline{u_{H^+}}(Q - q_{Na^+}(m,n)) + |z_{H^+}|u_{H^+}C_{H^+}(m,n) + |z_{A^-}|u_{A^-}C_{A^-}(m,n)} \quad (3)$$

## Cells and Bed Conductivities

Each cell conductivity (S/m) depends on the conductivity in the solid phase $\overline{\kappa}$ $(m,n)$ and in the liquid phase $\kappa(m,n)$. A relation proposed by Helfferich (9) is used to calculate $\kappa_{cell}$ $(m,n)$:

$$\kappa_{cell}(m,n) = \frac{a\kappa(m,n)\overline{\kappa(m,n)}}{d\kappa(m,n) + e\overline{\kappa(m,n)}} + b\overline{\kappa(m,n)} + c\kappa(m,n) \quad (4)$$

with a = 0.63; b = 0.01; c = 0.34; d = 0.95; e = 0.05, and:

$$\kappa(m,n) = \sum_i |z_i| C_i \lambda_i \quad \text{with i} = \mathrm{H}^+, \mathrm{Na}^+, \mathrm{A}^- \quad (5)$$

$$\overline{\kappa(m,n)} = \sum_i |z_i| q_i \lambda_{Ri} \quad \text{with i} = \mathrm{H}^+, \mathrm{Na}^+ \quad (6)$$

Each cell conductance is given by:

$$\Lambda_{cell}(m,n) = \kappa_{cell}\frac{S/N}{e/M} = \kappa_{cell}\frac{S_c}{e_c}$$

The conductance of a line is thus expressed by:

$$\frac{1}{\Lambda_{line}(n)} = \sum_{m} \frac{1}{\Lambda_{cell}(m,n)} \tag{7}$$

## I-U Relation

Lines of current are supposed to be perpendicular to the electrodes. Expressions which give U or I depend on the working mode which is chosen.

– Constant U: current of each line $I_{line}$ is calculated using Ohm's law.

$$I_{line}(n) = \Lambda_{line}(n)U \tag{8}$$

$$I_{global} = \sum_{n} I_{line} \tag{9}$$

– Constant I: U is calculated according to:

$$U = \frac{I_{global}}{\sum_n \Lambda_{line}}$$

Current of each line $I_{line}$ is then calculated using Equation (8).

## Mass Balances

As described on Fig. 2, on each cell (*m,n*), six terms can be defined:

- two inlet terms: convection coming from the cell (m,n − 1) and migration coming from the cell (m − l,n) for cations and from the cell (m + 1,n) for anions
- two outlet terms: convection towards cell (m,n + 1) and migration towards cell (m + 1,n) (cations) or (m − 1, n) (anions)
- two accumulation terms: in the liquid and the solid phase.

  The overall mass balance on each cell is therefore defined as follow:
- For $Na^+$

  $Na^+$ mass balance for cell (*m,n*) counts six terms:

$$\begin{aligned} &\mathrm{F_c C_{Na^+}(m,n-1)} + \frac{t_{\mathrm{Na^+}}(\mathrm{m}-1,\mathrm{n})I_{line}(n)}{96485.3 \times z_{\mathrm{Na^+}}} \\ &= \mathrm{F_c C_{Na^+}(m,n)} + \frac{t_{\mathrm{Na^+}}(\mathrm{m,n})I_{line}(n)}{96485.3 \times z_{\mathrm{Na^+}}} \\ &\quad + V_c\varepsilon \frac{dC_{\mathrm{Na^+}}(\mathrm{m,n})}{dt} + V_c \frac{dq_{\mathrm{Na^+}}(\mathrm{m,n})}{dt} \end{aligned} \tag{10}$$

where $V_c$ denotes cell volume and $\varepsilon$ bed porosity.

- For $A^-$ and AH

  There are only five terms, as long as there is no accumulation on solid phase because we are working with a cation exchange resin:

$$\begin{aligned} &\mathrm{F_c C_A(m,n-1)} + \frac{t_{A^-}(\mathrm{m}+1,\mathrm{n})I_{line}(n)}{96485.3 \times z_{A^-}} \\ &= \mathrm{F_c C_A(m,n)} + \frac{t_{A^-}(\mathrm{m,n})I_{line}(n)}{96485.3 \times z_{A^-}} \\ &\quad + V_c\varepsilon \frac{dC_A(\mathrm{m,n})}{dt} \end{aligned} \tag{11}$$

Considering the conservation of total weak acid concentration:

$$C_A(m,n) = C_{A^-}(m,n) + C_{AH}(m,n) \tag{12}$$

and the electroneutrality of the solution

$$C_{A^-}(m,n) = C_{H^+}(m,n) + C_{Na^+}(m,n) \tag{13}$$

It is not necessary to consider mass balances for HA and $H^+$ species.

## Cation Exchange Equilibrium

The liquid phase is assumed to be in equilibrium with the solid phase. In the case of a binary exchange of monovalent ions, action mass law leads to:

$$q_{Na^+} = \frac{QKC_{Na^+}}{C_{H^+} + KC_{Na^+}} \tag{14}$$

Where $K$ is the ion exchange $Na^+/H^+$ equilibrium constant and $Q$ the capacity of the ion exchange resin:

$$Q = q_{H^+}(m,n) + q_{Na^+}(m,n) \tag{15}$$

## Acid-Base Equilibrium

The acid dissociation equilibrium constant is:

$$K_a = \frac{C_{H^+}C_{A^-}}{C_{AH}} \tag{16}$$

Corresponding to the reaction $AH \leftrightarrow H^+ + A^-$

## Initial Conditions

Two types of initial conditions can be chosen: the bed can initially be uniformly on $H^+$ on $Na^+$ form. Due to the liquid-solid equilibrium assumption, the liquid phase must be in accordance to the resin form.

Thus, for $H^+$ form, a solution of the pure weak acid (without $Na^+$) is in equilibrium with the resin.

Initial conditions may be written:

$$C_{H^-}(m,n) = \frac{-K_a + \sqrt{K_a^2 + 4K_a C_{A^-+AH}}}{2}$$
$$C_{Na^+}(m,n) = 0$$
$$q_{Na^+}(m,n) = 0$$
$$C_{A^-}(m,n) = C_{H^+}(m,n)$$
$$C_A(m,n) = C_{initial}$$

For $Na^+$ initial form a solution of the salt $Na^+A^-$ (without $H^+$) is in equilibrium with the resin. Initial conditions may be written:

$$C_{Na^+}(m,n) = C_{initial}$$
$$q_{Na^+}(m,n) = Q$$
$$C_{A^-}(m,n) = C_A(m,n) = C_{Na^+}(m,n)$$

It can be noted that, for a given set of working parameters, identical steady state profiles are obtained for both type of initial conditions.

## Boundary Conditions

We first consider the cells (m = 1; n = 2,N) which are next to the membrane, on the anodic side. $Na^+$ flux which enters in the fixed bed on this side is considered to be null. Consequently Eq. (10) leads to:

$$\mathrm{F_cC_{Na^+}}(1,\mathrm{n}-1) + \mathrm{F}_c\mathrm{C_{Na^+}}(1,\mathrm{n}) + \frac{t_{\mathrm{Na^+}}(1,n)I_{line}(n)}{96485.3\ z_{\mathrm{Na^+}}} + V_c\varepsilon\frac{dC_{\mathrm{Na^+}}(1,n)}{dt} + V_c\frac{dq_{\mathrm{Na^+}}(1,n)}{dt}$$

Transversal $H^+$ inlet flux is proportional to the corresponding current $I_{line}$

$$F_cC_{H^+}(1,n-1) + \frac{I_{line}(n)}{96485.3z_{H^+}} = F_cC_{H^+}(1,n) + \frac{t_{H^+}(1,n)I_{line}(n)}{96485.3z_{H^+}} + V_c\varepsilon\frac{dC_{H^+}(1,n)}{dt} + V_c\frac{dq_{H^+}(1,n)}{dt}$$

If the permselectivity of the membrane is supposed to be ideal, no $A^-$ can cross this membrane.

Equation (11) leads to:

$$\mathrm{F_cC_A}(1,\mathrm{n}-1) + \frac{t_A-(2,n)I_{line}(n)}{96485.3z_{A^-}} = \mathrm{F_cC_A}(1,\mathrm{n}) + V_c\varepsilon\frac{dC_{A(1,n)}}{dt}$$

For the cells (m = M; n = 2,N) which are next to the cationic exchange membrane, on the cathodic side, Equation (11) leads to:

$$\mathrm{F_cC_A}(\mathrm{M},\mathrm{n}-1) = \mathrm{F_cC_A}(\mathrm{M},\mathrm{n}) + \frac{t_A-(M,n)I_{line}(n)}{96485.3z_{A^-}} + V_c\varepsilon\frac{dC_{A(M,n)}}{dt}$$

For the cells (m = 1, M; n = 1) which corresponds to the fixed bed inlet the concentrations are the feed concentrations:

$$C_{A^-}(m,1) = C_{Na^+}(m,1) = C_{feed}$$
$$C_{H^-}(m,1) = 0$$

## Numerical Method

The description of the model leads us to consider a differential/algebraic system. This system was solved via a modified DASSL (differential/algebraic system solver) method (10). DASSL uses Backward Differentiation Formula (BDF) methods (11) to solve a system of Differential/Algebraic Equations or Ordinary Differential Equations (ODEs). These methods are variable step size and variable order. The system of equations in DASSL is written in an implicit ODE form, e.g., $F(t,y,y') = 0$, where $F$, $y$, and $y'$ are vectors, $y'$ denotes the time derivatives of $y$, and initial values for $y$ and $y'$ are given.

The BDF methods used in DASSL require the solution of a large system of nonlinear equations of the form $F(t_n, y_n, \alpha_n y_n + \beta_n = 0$ for each time step, where $\alpha_n$ and $\beta_n$ are scalars which depend on the method and step size.

The system is solved by a modified Newton iteration such that each iteration solves a linear system $\mathrm{Ay_n^{(k+1)}} = \mathrm{b_n^{(k)}}$, where the matrix A is given by $\mathrm{A} = \alpha_n\frac{\delta \mathrm{F}}{\delta \mathrm{y}'} + \frac{\delta \mathrm{F}}{\delta \mathrm{y}}$.

DASSL also uses a banded direct solver to solve this linear system. Because the CPU cost to solve this linear system is proportional to the bandwidth of the matrix, the solver is quite efficient when the bandwidth of the matrix is relatively small. Different moving mesh strategies result in different bandwidths, which is a very important factor when considering the efficiency of the method. A compromise between the required precision and calculation time led to work with M = N = 15. Details of the DASSL method can be found elsewhere (12).

## Global Parameters

Resolution of the previous system enables to evaluate several parameters:

– Outlet concentration (at a given time):

$$C_{i,out} = \frac{1}{M}\sum_{m=1}^{m=M} C_i(m,N)$$

– Solid phase average concentration:

$$q_{i,mean} = \frac{1}{NM}\sum_{n=1}^{n=N}\sum_{m=1}^{m=M} q_i(m,N)$$

– Current efficiency for $Na^+$ removal:

$$R_f = \frac{\left(C_{Na+feed} - \frac{1}{M}\sum_{m=1}^{m=M} C_{Na+}(m,N)\right)}{I/96485.3}F$$

Furthermore, the knowledge of the cell concentrations enables the determination of the concentration profiles in both longitudinal and transversal directions.

## RESULTS AND DISCUSSION

Numerical values used for the simulations arc gathered in Tables 1 and 2.

### Salt to Acid Conversion

Conversion is defined as the ratio of acid concentration in the output flow to the salt concentration in the feed. Conversion varies during the transient state from initial conditions to a constant value at steady state. Figure 3 shows experimental conversion at steady state versus the feed flow rate at constant current for two current density values: 375 $Am^{-2}$ (EDI) (I = 1.5 A) and 1000 $Am^{-2}$ (EDI-BM) (I = 4A). Two groups of points can clearly be observed, depending on the current density value. In order to compare these results, a reduced flow rate $F_{red}$ is introduced. It is defined as the ratio of the experimental flow rate F over the maximum flow rate $F_{100\%}$ which would enable 100% conversion, in the case of 100% current efficiency:

$$F_{red} = \frac{F}{F_{100\%}}$$

Where $F_{100\%}$ is be expressed as:

$$F_{100\%} = \frac{1}{z_{Na+}C_{Na+feed}\ 96485.3}$$

TABLE 2
Ion exchange bed data used for the simulations

| | |
|---|---|
| Capacity of the ion exchange resin Q | 1.79 eq · $L^{-1}$ |
| Ion exchange $Na^+/H^+$ equilibrium constant K | 1.56 |
| Bed porosity $\varepsilon$ | 0.4 |

As shown on Fig. 4, using this dimensionless number enables to obtain a single curve representation. Furthermore, Fig. 4 shows a good agreement between experimental and simulated conversion. As a result, modelling enables to obtain helpful tools to determine working parameters: for a given EDI configuration, calculation of conversion rate versus reduced flow rate can be achieved. This representation enables to determine the maximum flow rate to be used if a minimal conversion rate is required. It can be noticed that the conversion rate has a strong nonlinear dependence upon the reduced flow rate which makes it difficult to estimate working parameters without modelling tools.

### Transient State and Na Breakthrough Curve

Figure 5 gives the experimental EDI-BM Na breakthrough curve in the case of the following conditions: sodium lactate feed concentration 123 mol $m^{-3}$, I = 1000 A $m^{-2}$, F = 19.6 mL $mn^{-1}$ ($F_{red} \approx 1$), resin initially on $H^+$ form.

Three domains can be identified. In the first (t < 1 500 s) a part of the inlet sodium migrates towards the cathodic compartment whereas the other part is fixed on the resin and exchanged for $H^+$ ions resulting in lactic acid: thus no sodium exits the bed and the lactic acid is almost pure in the effluent. In the second domain, there is no more capacity for sodium to fix and the breakthrough occurs. The effluent contains lactic acid with sodium lactate. These two first parts correspond to the transient state. After that the concentration remains constant: steady state is attained. The composition of the resin no more varies. The concentration is 16.8 mol $m^{-3}$ compared to 123 mol $m^{-3}$ in the feed.

TABLE 1
Molar conductivity and mobility values used for the simulations

| | Liquid phase | | Solid phase | |
|---|---|---|---|---|
| | Conductivity $\lambda$ S $m^2$ $mol^{-1}$ | Mobility $u$ $m^2$ $V^{-1}$ $s^{-1}$ | Conductivity $\lambda_R$ S $m^2$ $mol^{-1}$ | Mobility $\bar{u}$ $m^2$ $V^{-1}$ $s^{-1}$ |
| $H^+$ | $35 \times 10^{-3}$ | $36 \times 10^{-8}$ | $1.92 \times 10^{-3}$ | $19.9 \times 10^{-9}$ |
| $Na^+$ | $5 \times 10^{-3}$ | $5.19 \times 10^{-8}$ | $5.9 \times 10^{-4}$ | $6.1 \times 10^{-9}$ |
| Lactate ion $A^-$ [13] | $4 \times 10^{-3}$ | $4.15 \times 10^{-8}$ | | |

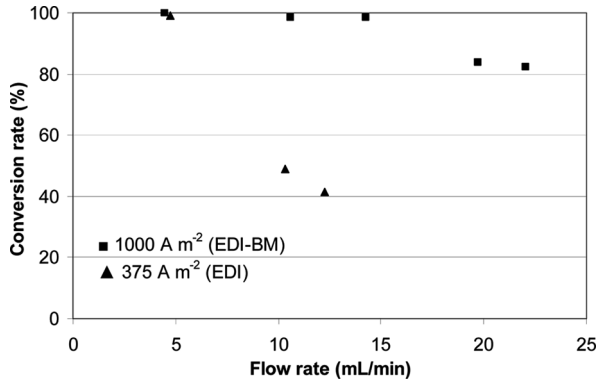


FIG. 3. Flow rate influence on conversion.

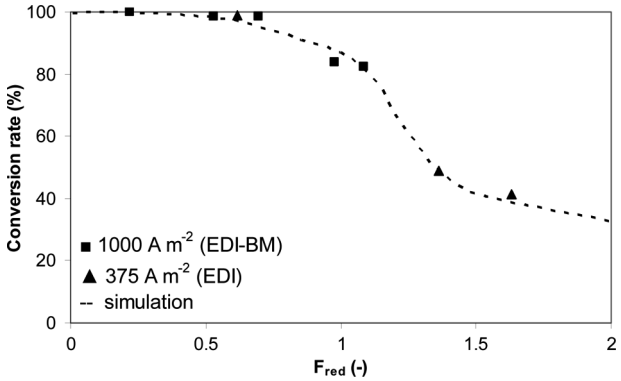


FIG. 4. Comparison of simulated and experimental electrodeionization conversion.

Thus the conversion of lactate to lactic acid is in this case of 86%.

## 2D Concentration Profiles Representations

Simulated concentration profiles in liquid and solid phases are given in Figs. 6 and 7, respectively, for the same conditions than in section 4.2.

Several observations can be made:

- t = 1000 s: unsteady state. Resin sodium content is increasing with time. Outlet sodium concentration is near to zero. Conversion is total.
- t = 3000 s: unsteady state. Breakthrough point has been reached. Na outlet concentration is not null. Resin has however not yet its final state. A part of the capacity is still available for exchange.
- t = 6000 s: steady-state. Outlet concentration remains constant, as well as the resin state in the compartment. Near bed outlet, resin is in equilibrium with the outlet effluent and is not saturated.

These 2D concentration profile representations make it easier to understand the way to optimize this kind of system: working parameters should permit to maximize the feed flow rate, still keeping in steady-state the front in the column, in order to respect constraints regarding the outlet leakage concentration admitted. Using an analogy with the classical ion exchange breakthrough point definition, an "EDI steady-state breakthrough point" can be defined. This analogy involves a spatial/temporal transposition. The spatial position of this point depends on many parameters such as the inlet concentration, feed flow rate,

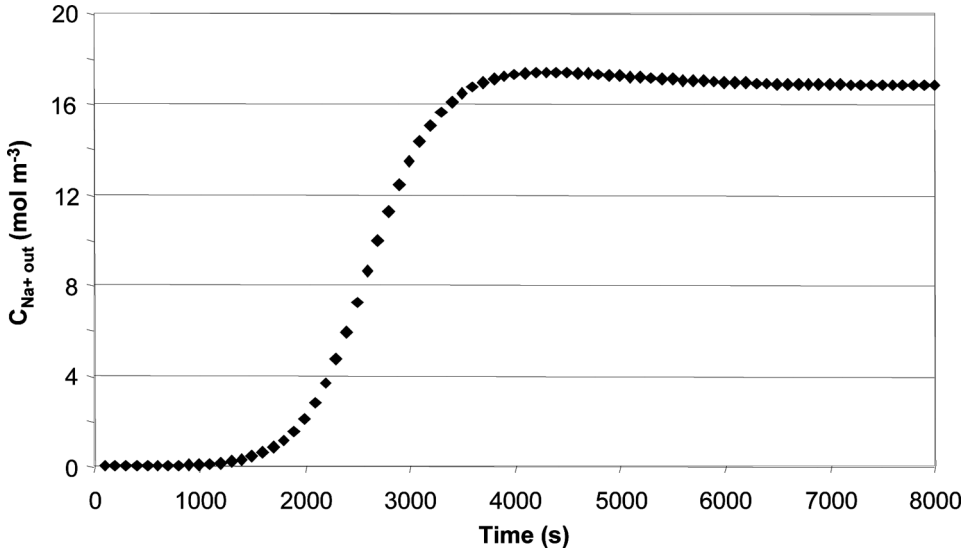


FIG. 5. EDI-BM Na breakthrough curve sodium lactate inlet concentration 123 mol $m^{-3}$, I = 1000 A $m^{-2}$, F = 19.6 mL $mn^{-1}$ ($F_{red}$ = 1), resin volume 60 mL initially under $H^+$ form (Q = 1790 eq $m^{-3}$).

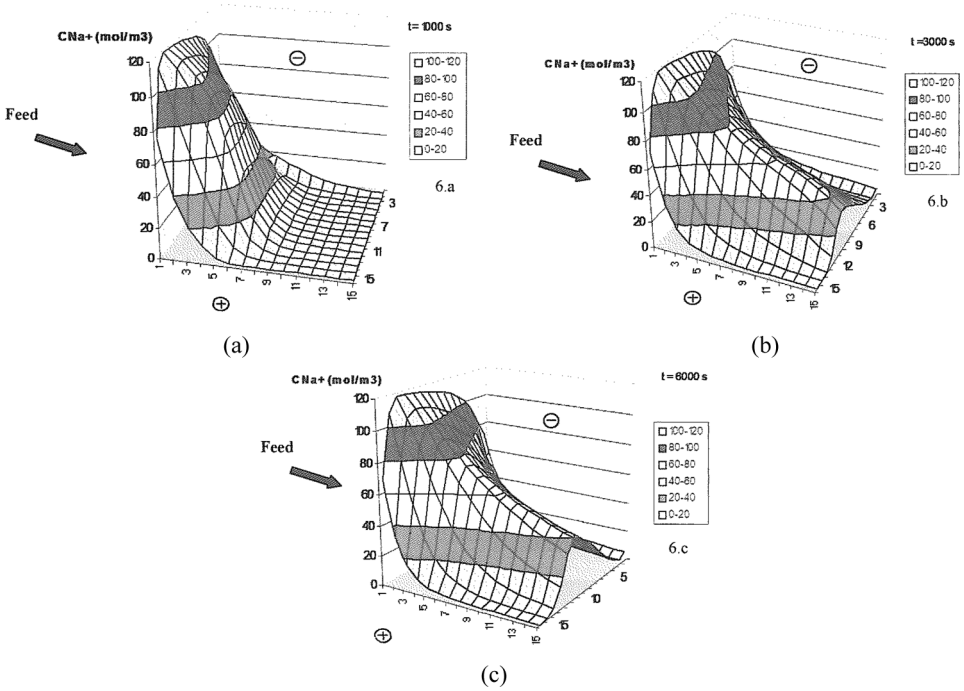


FIG. 6. 2D Na solution concentration profiles for EDI-BM (t = 1000 s (Fig. 6a), t = 3000 s (Fig. 6b) and t = 6000 s (Fig. 6c)).

current (or potential) applied, solution and resin electrical conductivity. For a given application, these parameters must be adjusted such that $Na^+$ exit concentration is limited to a specified value.

Another observation can be made regarding the obtained profiles, showing a maximum of $Na^+$ concentration in the middle width cell. This is different from classical EDI of water and is probably due to the weak

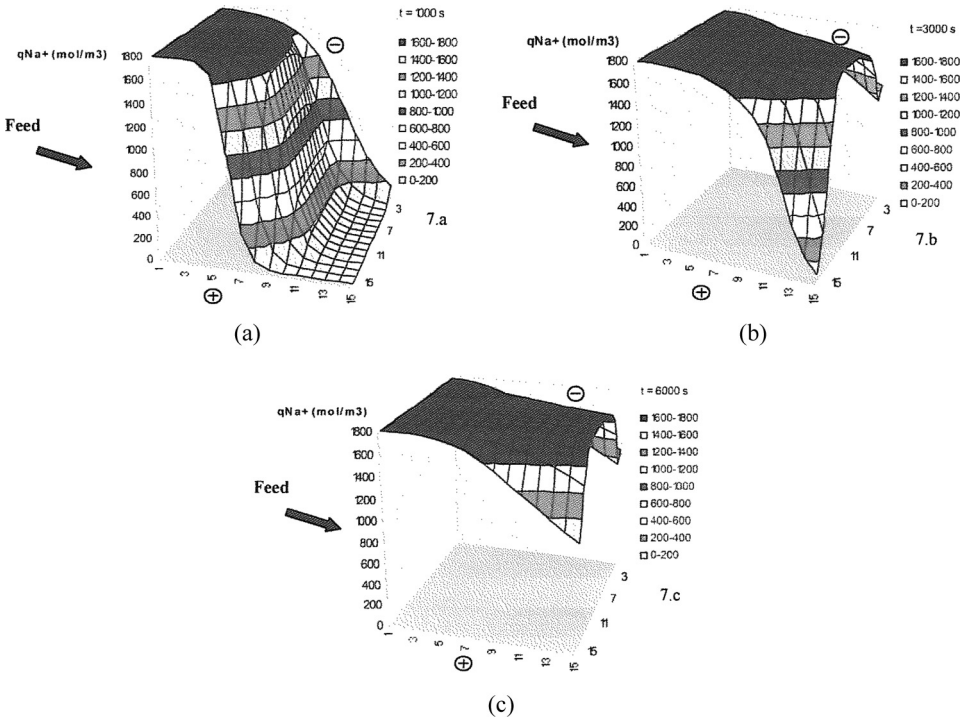


FIG. 7. 2D Na resin concentration profiles for EDI-BM (t = 1000 s (Fig. 7a), t = 3000 s (Fig. 7b) and t = 6000 s (Fig. 7c)).

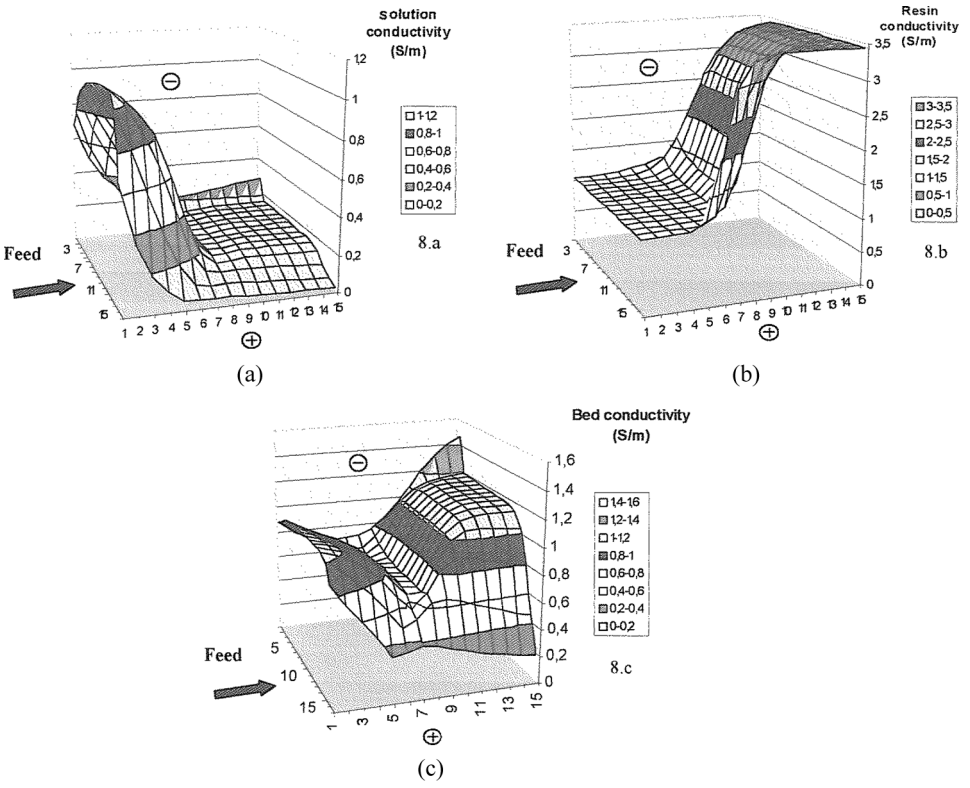


FIG. 8. EDI-BM conductivity profiles at t = 1000 s (a) Solution conductivity $\kappa_{solution}$; (b) resin conductivity $\overline{\kappa}_{resin}$; (c) bed conductivity $\kappa_{cell}$.



acid. Let us consider the curves at t = 1000 s. It can be observed on Fig. 7a that, at the bed inlet, the resin is almost saturated under $Na^+$ form, on all the width in a homogeneous way. However, it can be noticed on Fig. 6a that the $Na^+$ concentration in solution decreases on the anodic and on the cathodic side and thus goes to a maximum in the middle width cell.

On the anodic side, the entering $H^+$ convert $A^-$ into AH and $Na^+$ ions migrate towards cathodic side. On the opposite, near the cathodic membrane, conversion of $A^-$ into AH hardly takes place, especially when the resin is saturated under $Na^+$ form. Therefore, the unconverted $A^-$ can migrate towards the anodic side. This phenomenon has got three consequences:

- a decrease of the solution normality, thus a decrease of $Na^+$ concentration; the solution conductivity profiles observed on Fig. 8a seems to corroborate this statement.
- A change of the total concentration $C_A$ of the acid (undissociated AH and anion $A^-$). It can be shown that an increase of $C_A$ leads to an increase of selectivity of $Na^+$.
- a competition effect for the current transport ($A^-$/$Na^+$).

## Specific Conductivity and Current Distribution

Previous observations bring us to consider the resistivity aspects. Let us consider the same operation than that described previously. Conductivity profiles can be calculated from concentration profiles. Figure 8 shows respectively the solution, the resin, and the bed conductivity profiles, for t = 1000 s (nonsteady-state). Several observations can be made:

- Solution conductivity is high as long as sodium lactate is not converted near the bed inlet. As conversion proceeds, sodium lactate is converted into lactic acid, which is weakly dissociated, and a progressive conductivity decreasing can be observed along the bed.
- With regard to resin conductivity, the evolution is the other way around, as the resin conductivity is higher under $H^+$ than under $Na^+$ form.
- Bed conductivity combines both the previous effects: two conductive zones can be observed respectively, near the inlet and near the outlet of the cell. An intermediary zone, corresponding to the front position, presents a higher resistivity. Modelling enables clear observation of this distribution, which is not really intuitive. From this

observation there appears to be an advantage of EDI over ED. Indeed, without any resin in the compartment, the conductivity profile would be the solution one, which leads to a preferential current in the high conductivity zone. The EDI bed conductivity profile enables to tend towards a more uniform current distribution.

## CONCLUSION

The modelling of a weak acid conversion in an EDI cell has been described. Simulations supply results which agree well with experiments. A reduced flow rate $F_{red}$, defined as the ratio of the experimental flow rate over the maximum flow rate which would enable 100% conversion, in the case of 100% current efficiency, has been introduced. Steady-state conversion rate appears to be a function of this dimensionless parameter. The modelling leads to numerical determination of this dependency, which constitutes a helpful tool to determine working parameters. Besides a notion of ''EDI steady-state breakthrough point'' position has been introduced. For a given inlet concentration, current (or potential) and flow rate must be chosen to optimize this point position, enabling to obtain the required purity, while insuring a rationalized bed utilization.

## NOTATION

| | |
|---|---|
| $C$ | liquid phase concentration ($\mathrm{mol\,m^{-3}}$) |
| $e$ | width of the packed bed (m) |
| $F$ | feed flow rate ($\mathrm{m^3\,s^{-1}}$) |
| $I$ | current (A) |
| $m$ | cell line number (−) |
| $n$ | cell column number (−) |
| $q$ | resin phase concentration ($\mathrm{mol\,m^{-3}}$) |
| $S$ | contact area of one side of the packed bed with membrane ($\mathrm{m^2}$) |
| $t_\mathrm{i}$ | transport number (−) |
| $t$ | time (s) |
| $U$ | cell voltage (V) |
| $u_\mathrm{i}$ | mobility of an individual ion species in the liquid phase ($\mathrm{m^2\,s^{-1}\,V^{-1}}$) |
| $\overline{u}_i$ | mobility of an individual ion species in the resin phase ($\mathrm{m^2\,s^{-1}\,V^{-1}}$) |
| $z_\mathrm{i}$ | ionic valence |

### Subscripts

| | |
|---|---|
| c | corresponding to one cell |

### Greek Letters

| | |
|---|---|
| $\varepsilon$ | bed porosity (−) |
| $\kappa$ | Electrical conductivity of the liquid ($\mathrm{S\,m^{-1}}$) |
| $\overline{\kappa}$ | Electrical conductivity of the solid ($\mathrm{S\,m^{-1}}$) |
| $\kappa_b$ | Electrical conductivity of the bed ($\mathrm{S\,m^{-1}}$) |
| $\lambda_i$ | Molar conductivity in the liquid phase ($\mathrm{S\,m^2\,mol^{-1}}$) |
| $\lambda_{Ri}$ | Molar conductivity in the resin phase ($\mathrm{S\,m^2\,mol^{-1}}$) |
| $\Lambda$ | Conductance ($\mathrm{A\,V^{-1}}$) |

### Abbreviations

| | |
|---|---|
| BM | bipolar membrane |
| CEM | cation exchange membrane |
| ED | electrodialysis |
| EDBM | bipolar membrane electrodialysis |
| EDI | electrodeionization |
| EDI-BM | electrodeionization using bipolar membrane |
| IEX | Ion Exchanger |

## REFERENCES


1. Thate, S.; Specogna, N.; Eigcnbergcr, G. (1999) A comparison of different EDI concepts used for the production of high-purity water. *Ultrapure Water*, 16 (8): 42–56.
2. Bailly, M. (2000) Strategic de dimensionnement de procédés de production d'acides organiques intégrant des étapes électromembranaires, Thése de doctorat, Université Paul Sabatier de Toulouse.
3. Bailly, M. (2002) Production of organic acids by bipolar electrodialysis: realizations and perspectives. *Desalination*, 144: 157–162.
4. Roux de Balmann, H.; Casademont, E. (2006) Electrodialyse, Techniques de l'ingénieur, J2: 840.
5. Roux de Balmann, R.; Bailly, M.; Lutin, F.; Aimar, P. (2002) Modelling of the conversion of weak organic acids by bipolar membrane electrodialysis. *Desalination*, 149: 399–404.
6. Koter, S. (2007) Modeling of weak acid production by the EDB method. *Separation and Purification Technology*, 57: 406–412.
7. Verbeek, H.M.; Furst, L.; Neumeister, H. (1998) Digital simulation of an electrodeionization process. *Computers Chem. Engng.*, 22: S913–S916.
8. Thate, S. (2002) *Untersuchung der elektrochemischen Deionisation zur Reinstwasserherstellung*. Ph.D. Thesis, Stuttgart Univ., Institut für Chemische Verfahrenstechnik, Germany Diss ISBN 3-89722-9U-0.
9. Hellferich, F. (1995, reedition 1962) *Ion Exchanges*; Dover Publications: New York.
10. Petzold, L.R. (1983) *A Description of DASSL: A Differential/Algebraic Svstem Solver*; Stepleman, R.S., et al., editors. Scientific Computing, Amsterdam: North-Holland.
11. Gear, C.W. (1971) *Numerical Initial Value Problems in Ordinary Differential Equations*; Prentice-Hall: Englewood Cliffs, NJ.
12. Brown, P.N.; Hindmarsh, A.C.; Petzold, L.R. (1994) Using Krylov methods in the solution of large-scale differential-algebraic systems. *SIAM J. Sci. Comput.*, 15: 1467–88.
13. Lide, D.R.; Frederikse, H.P.R. (1994) *CRC Handbook of Chemistry and Physics*, 74th Edition; CRC Press: Boca Raton, FL.